Activation of recombinant mouse acetylcholine receptors by acetylcholine, carbamylcholine and tetramethylammonium

Yinong Zhang, Jian Chen and Anthony Auerbach*

Department of Biophysical Sciences, State University of New York at Buffalo, Buffalo, NY 14214, USA

1. The kinetic properties of cloned mouse embryonic nicotinic acetylcholine receptors (AChRs) expressed in HEK 293 cells or *Xenopus* oocytes were examined using high concentrations of acetylcholine (ACh), carbamylcholine (CCh), or tetramethylammonium (TMA). The rate constants of agonist binding and channel gating were estimated by fitting kinetic models to idealized open and closed intervals over a range of agonist concentrations.

2. Once doubly liganded, TMA-activated receptors open at $\sim 3000\ s^{-1}$. The equilibrium binding constants for TMA are 525 and 12 800 μM. Doubly liganded CCh-activated receptors open at $\sim 11\,500\ s^{-1}$; the equilibrium binding constants for this agonist are 14 and 570 μM. If we assume that doubly liganded, ACh-activated receptors open at $60\,000\ s^{-1}$, then the equilibrium binding constants for ACh are 20 and >650 μM, similar to those for CCh. For all three agonists the higher affinity site both binds and releases agonists more slowly than does the lower affinity site.

3. ACh and CCh bind to the two sites equally rapidly, at $\sim 2 \times 10^7$ and $4 \times 10^7\ M^{-1}\ s^{-1}$ at the first and second binding sites, respectively. Compared with ACh, the TMA association rate is ~ 100 times slower at the first binding site, and ~ 30 times slower at the second binding site. These results indicate that at both binding sites the association rate of TMA is not limited by diffusional or steric factors.

4. All three agonists dissociate from the receptor binding sites at similar rates. The dissociation rate for all agonists was ~ 40 times slower at the first binding site than at the second. These results suggest that the interaction of the quarternary amine moiety with the receptor determines the rate of release of the agonist, and that the nature of this interaction is quite different at the two binding sites.

5. Although the channel opening rates for the three agonists varied ~ 20-fold, the channel closing rates were not strongly agonist dependent, and varied less than 3-fold. We speculate that the ester moiety of the agonist promotes both rapid binding and fast opening of the ligand receptors, and that interactions of the quarternary amine moeity of the agonist with the receptor determine the channel closing rate constant.

Studies of nicotinic acetylcholine receptor (AChR) activation properties have been carried out at the single-channel level for receptors from several different species, including mouse (Sine & Steinbach, 1987; Jackson, 1988), frog (Colquhoun & Sakmann, 1985; Auerbach, 1993), and *Torpedo* (expressed in mouse fibroblasts; Sine, Claudio & Sigworth, 1990). These studies have produced a consensus with regard to some features of the activation process (reviewed by Lingle, Maconochie & Steinbach, 1992). (1) A receptor usually binds two agonist molecules before opening. (2) The association and dissociation of ACh are fast and allow a rapid onset and termination of the synaptic response (discussed by Jackson, 1989). (3) The two agonist binding sites are not equivalent, i.e. they have different equilibrium dissociation constants. (4) Once doubly liganded with ACh, a receptor opens within 10–30 μs and closes after a few milliseconds. Quantitative estimates of the activation parameters – such as the acetylcholine association rate constants and the channel opening rate constant – have, however, varied considerably, in part because different experimental and analytical methods were used.

Specific interactions of the agonist with the receptor protein influence the rate constants of association, dissociation,

* To whom correspondence should be addressed.

opening and closing. One way to probe the molecular mechanisms that underly the activation reaction is to examine these rate constants for ACh analogues. The activation parameters for several nicotinic agonists have been investigated at the level of single channels, both in terms of rate constants (Colquhoun & Sakmann, 1985; Sine & Steinbach, 1987) and equilibrium dose–response curves (Marshall, Ogden & Colquhoun, 1991). These studies suggest that agonists differ mostly in their binding, rather than gating, parameters.

In this paper we report the binding and gating properties of an AChR that is commonly used in mutagenesis studies: mouse wild-type, embryonic (made of α-, β-, γ- and δ-subunits) receptors expressed in either oocytes or via transfection of human embryonic kidney (HEK) 293 cells. We studied the agonists acetylcholine, carbamylcholine and tetramethylammonium. The results indicate that (1) the two AChR binding sites differ more than 20-fold in their equilibrium affinities, largely because of a difference in dissociation rates, (2) the rate of agonist association is not limited by diffusion or by steric interactions with the receptor, i.e. an agonist must cross one or more energy barriers before binding to its docking site, and (3) interactions of the ester moiety of the agonist with the receptor speeds both association and channel opening but has relatively little effect on the rates of channel closing and agonist dissociation.

METHODS

Expression systems

The cDNA clones coding α-, β-, γ- and δ-subunits of mouse wild type nAChR used in the transfection of HEK 293 cells (ATCC CRL 1573) were constructed in either the pRBG4 (Sine, 1993) or pCDNAIII (Invitrogen, San Diego, CA, USA). The stock HEK 293 cells were treated with 0·25% Trypsin–EDTA (Gibco) and the dispersed cells were suspended in fresh media. The cells were then plated in 35 mm tissue culture dishes at a density of about 5×10^5 cells per dish. The HEK 293 cells were maintained at 37 °C in culture (89% Dulbecco's modified Eagle's medium (DMEM), 10% fetal bovine serum, 50 u ml^{-1} penicillin and 50 μg ml^{-1} streptomycin, pH 7·4) and subcultured 10–12 h before transfection.

A standard calcium phosphate precipitation method was used in the transfection of HEK 293 cells (Ausubel, 1992). The cDNAs coding α-, β-, γ- and δ-subunits were premixed at a ratio of 2:1:1:1 and 3·5 μg of the DNA mixture was added to each 35 mm dish. The cells were maintained (37 °C, 5% CO_2) for 5–20 h, after which time the medium was changed. Electrical recordings started 2 days later.

For mRNA preparation and injection of oocytes, healthy stage VI oocytes were extracted from adult *Xenopus laevis* that had been anaesthetized with MS222 (Sigma) and the follicular envelopes were removed by incubating oocytes in a Ca^{2+}-free solution (mM: 115 NaCl, 1·5 KCl, 10 Hepes, pH 7·4) containing 1 mg ml^{-1} collagenase. The cDNA clones coding mouse wild type nAChR subunit α, β, γ and δ were generously provided by Dr James Patrick (Baylor Medical College, Houston, TX, USA). The plasmids were linearized with HindIII (α-, β- and δ-subunits) or EcoRI (γ-subunit) and transcribed with SP6 RNA polymerase. mRNAs were resuspended in nuclease-free water at concentrations of 200 (α) or 100 ng μl^{-1} (β, γ and δ) and mixed at a ratio of 2:1:1:1 (by weight). Each de-folliculated oocyte was injected with 50 nl of this mixture. The injected oocytes were stored individually in 60% L-15 and in a 48-well tissue culture cluster. Electrical recording started 2 days later.

Electrophysiology and solutions

The standard patch pipette solution for both HEK 293 cells and oocytes was (mM): 115 NaCl, 10 Hepes–NaOH, 1 $CaCl_2$, 2 KCl, pH 7·4. This was also used as the bath solution for oocytes, but for HEK 293 cells the bath solution was (mM): 137 NaCl, 4·3, Na_2HPO_4, 1·4 KH_2PO_4, 1 $CaCl_2$, 2·7 KCl, pH 7·4. The temperature was 19–20 °C (oocytes) or 22–23 °C (HEK 293 cells). The membrane potential was −90 mV, and the single-channel amplitude (no channel block) was 3–5 pA. All data were from cell-attached patches. All reagents were from Sigma.

Single-channel analysis

The first stages of analysis were similar to those described in Auerbach (1993). Single-channel currents were filtered at 20 kHz (−3 dB; 8-pole Bessel) and stored on a digital data recorder (94 kHz sampling rate; Instrutech VR-10, New York). The data were played back into a DOS-based computer either as an analog signal with redigitization at 50 kHz or by direct transfer (at 47 or 94 kHz) via a digital interface. Currents were idealized after digital low-pass filtering (Gaussian filter, cut-off frequency (f_c) = 2 kHz) using a half-amplitude threshold-crossing algorithm. After fitting a log bin width histogram of all closed interval durations to the sum of three to five exponentials, clusters of openings were defined by a critical time τ_{crit}, which was 3–5 times longer than the predominant closed time component. τ_{crit} ranged from ~500 ms at 2 μM to ~0·2 ms at 1 mM ACh.

The kinetics of both natural and expressed AChR are heterogeneous (Auerbach & Lingle, 1986; Naranjo & Brehm, 1993); thus for each patch we selected a subset of currents that were apparently homogeneous in their activation characteristics. Clusters were examined for several properties – amplitude, open and closed interval durations, probability of being open (P_{open}), number of open intervals, number of openings per millisecond, and baseline noise standard deviation – and those that were within 2 S.D. of the means for all of these properties, and were >100 ms in duration, were extracted and saved for further analysis. The cluster P_{open} was calculated from the idealized interval durations using an equal number of open and closed intervals (Auerbach, 1993).

As an example of the selection process we can follow the pruning of a typical record (5 μM ACh). The original digitized record was 685 s and contained 677 openings that were long enough (>0·25 ms) to have amplitudes that were well defined at the 2 kHz analysis bandwidth. The mean amplitude of these open intervals was 4·1 pA and their mean duration was 5·14 ms. The overall P_{open} for the record, including periods when all receptors were desensitized, was 0·005. Closed intervals (n = 967, including those <0·25 ms) could be described by three exponentials: τ_1 = 0·49 ms (f_1 = 0·09), τ_2 = 25·6 ms (f_2 = 0·58) and τ_3 = 2000 ms (f_3 = 0·33), where τ is the time constant and f is the fractional area. From these values τ_{crit} was set to 125 ms (5 times τ_2), and seventeen clusters were defined that were >100 ms in duration (mean, 618 ms) and had >10 open intervals (mean, 28·3). In these clusters the mean open interval lifetime was 5·6 ms, the mean closed interval lifetime was 17·0 ms, the mean P_{open} was 0·27 and

the mean open interval amplitude was 4·07 pA. From these clusters we selected a subset of twelve that had P_{open} values between 0·15 and 0·35. In these clusters (mean duration, 680 ms) the mean open interval lifetime was 5·4 ms, the mean closed interval lifetime was 18·4 ms (described by two exponentials: $\tau_1 = 0{\cdot}27$ ms ($f_1 = 0{\cdot}31$), $\tau_2 = 26{\cdot}3$ ms ($f_2 = 0{\cdot}69$)), and the mean P_{open} was 0·23. Of the 677 openings in the original record 309 (from 12 clusters) were selected for detailed kinetic analysis.

The inverse time constant of the slowest intracluster closed interval component was defined as the effective opening rate, or β', and was obtained by fitting the cluster closed interval histogram to sums of two to three exponentials. This time constant (26·3 ms in the example file) reflects sojourns in the set of vacant and liganded closed states of the activation reaction and is the microscopic analogue of the time constant of the rising phase of the current that develops in response to a step increase in the agonist concentration.

The selected current clusters were idealized a second time by a half-amplitude method, this time at a higher bandwidth ($f_c = 5$ kHz) and using a correction for the effects of filtering on duration (eqn (17) of Colquhoun & Sigworth, 1983). The detection threshold was adjusted according to the mean open channel amplitude of each cluster. Events shorter than a specified 'dead time' ($\tau_{dead} = 0{\cdot}18/f_c$) were eliminated from the idealized record by fusing them with the previous interval. The rate estimates were obtained by fitting the list of idealized open and closed interval durations using a simplex algorithm, with the log likelihood (LL) computed on an interval-based maximum likelihood method (Horn & Lange, 1983; Ball & Sansom, 1989) with a first-order correction for missed events (Roux & Sauve, 1985). To check that the rates described the binned data, after convergence open and closed interval duration probability density functions (PDFs) were computed from the fitted parameters and were superimposed on the log-binned open and closed interval duration histograms (Sigworth & Sine, 1987).

Next, the fitted rates were used to idealize the data at a higher bandwidth ($f_c = 6$–12 kHz) using the Viterbi algorithm (Forney, 1972; Chung, Moore, Xia, Premkumar & Gage, 1990). Given a finite state Markov model that is defined by states (each of which has a characteristic amplitude and noise variance), and transition rates between the states, this algorithm generates the most likely state sequence in the digitized current record. The noise variance was assumed to be Gaussian and white, and was estimated from a 3 ms segment of baseline that immediately preceded the first opening in each cluster. At very high ACh concentrations, where the open channel noise is large because of channel block, the noise variance was estimated from a 1 ms segment of open channel current that immediately followed the first opening transition in each cluster, and the open state(s) of the model were assigned this higher variance. The resulting state sequence for the final set of clusters was condensed into a list of open and closed interval durations by assigning an open or closed class designator to each state of the model. This list was subjected to a second round of fitting by the interval log likelihood method, with a τ_{dead} of 15 or 25 μs, depending on f_c. The rate constant estimates obtained by this round of fitting are the final rates reported in the text and tables.

Idealization with the Viterbi algorithm or maximum likelihood fitting of the idealized interval durations generates a log likelihood (LL) for each cluster. These LL values, normalized either on the basis of cluster duration (Viterbi method) or number of events (interval method), were used as a final screen for heterogeneity in the kinetic properties of clusters. Although the absolute values of the normalized cluster LL varied with the noise variance (Viterbi method) or the event duration (interval method), typically the normalized LL values were in the ranges -80 to -30 ms^{-1} or 3–6 per event. Clusters that had normalized LL values less than these minimum values were excluded from the final rate estimates.

For every fit, positive and negative error limits on each rate were estimated by a 1/2 likelihood interval method (Colquhoun & Sigworth, 1983). Each parameter was moved to some value different from its optimum and all other rate constants were allowed to vary until a new maximum log likelihood was reached. By bisection, a positive S.E.M. of the parameter was defined as the value that produced a maximum LL that was 0·5 lower than the global maximum. Negative S.E.M. were estimated by searching values below the global optimum. In this way, a LL surface in the vicinity of each parameter was estimated. All modelling computations were on IBM RS/6000 workstations.

Returning to the example 5 μM ACh file, at high bandwidth ($f_c = 8$ kHz) the mean baseline noise for the selected clusters was 0·78 pA (range, 0·66–0·94 pA) and the mean cluster LL (Viterbi idealization) was $-49{\cdot}5$ ms^{-1} (range, -38 to -68). These ranges indicate that the set of clusters was homogeneous with regard to noise and model parameters. After the final round of fitting noise-free intervals by the interval maximum likelihood method the mean cluster LL was 5·32 per event (range, 4·45–5·87). These values, too, indicate that the clusters were homogeneous and well described by the model. When fitted to model 3 (CCOC) the rate constants (± error limits) were: $k_{+1} = 36\ \mu$M^{-1} s^{-1} (+5·6, −4·4), $k_{-1} = 1629$ s^{-1} (+356, −331), $k_{+2}{}^* = 120\ \mu$M^{-1} s^{-1} (+34, −26), $\alpha^* = 112$ s^{-1} (+7·4, −7·0), $k_{+g} = 462$ s^{-1} (+29, −27), and $k_{-g} = 26511$ s^{-1} (+1553, −1450). These rate constants predict an open interval duration distribution ($\tau_{dead} = 25\ \mu$s) that can be described by a single exponential ($\tau = 2{\cdot}92$ ms) and a closed interval duration distribution that has three exponential components: $\tau_1 = 0{\cdot}039$ ms ($f_1 = 0{\cdot}52$), $\tau_2 = 0{\cdot}42$ ms ($f_2 = 0{\cdot}10$) and $\tau_3 = 22{\cdot}1$ ms ($f_3 = 0{\cdot}37$).

Intervals excluded from the analysis

Two kinds of event were observed that were not explicitly included in the activation models that we used. First, in oocytes, sojourns in a substate with an amplitude that was smaller than that of the main open state were sometimes apparent (but were rarely seen in HEK 293 cells). We handled this event by adding an extra state, A_2S, to the idealization model used in the Viterbi algorithm. The properties of this substate were first determined by an analysis of four patches: amplitude = 0·66 of the main state, lifetime = 6 ms, frequency = 20 s^{-1} of open time. Sojourns in A_2S were assigned an 'open' classification. The inclusion of this substate effectively increased the dead time, which in oocyte experiments was set to 55 μs.

The second type of event that was not included in the activation schemes was a sojourn in a closed state that was only apparent at high (>50 μM) ACh concentrations. This state may be a relatively short-lived desensitized state. In three files at 0·1–5 mM ACh, the properties of this closed state were determined: lifetime = 4·5 ms, frequency = 2 s^{-1} of open time. We eliminated these events by assigning τ_{crit} values that were sufficiently short to exclude them.

Calculations from the rate constants

After fitting, several 'macroscopic' channel behaviours were computed from the rate constants. First, open and closed interval duration probability density functions were computed using the

rate matrix (modified by the system dead time), and these were compared with log-binned histograms. Second, a dose–response curve was computed from the rate matrix (modified by the system dead time) and superimposed on the single-channel P_{open} profiles. As a final check, the rate constants obtained from single-channel modelling were used to fit experimental binding curves. In addition to the activation rate constants, two parameters were required to generate these curves – the equilibrium constant for binding to desensitized receptors (K_r; assumed to be the same for each site) and the equilibrium constant for the desensitization of a vacant receptor (M). The fraction of bungarotoxin remaining bound (Y) in the presence of competing agonist (x) is (modified from Sine, Quiram, Papanikolaou, Kreienkamp & Taylor, 1994):

$$Y = 1 - \{(Ax + Bx^2)/(1 + M + 2Ax + Bx^2)\},$$

$$A = 1/2K_1 + M/K_r,$$

$$B = 1/K_1K_2 + M/K_r^2 + \Theta/K_1K_2,$$

where Θ is equal to β/α. For the curves shown in Fig. 5, K_r was the only free parameter of the fit; M was fixed at 10^{-4} (Sine *et al.* 1994). Note that this function is dominated by M and K_r and is thus not a critical test of the equilibrium dissociation constants K_1 and K_2. However, using the activation equilibrium constants obtained by kinetic modelling to account for equilibrium occupancy results shows that both sets of observations are consistent.

RESULTS

Basic characteristics of clusters

At high concentrations of agonist, acetylcholine receptor (AChR) channel currents occur in clearly defined clusters. Between clusters, the receptors in the patch are desensitized. Each cluster occurs when one receptor has returned from being desensitized and makes transitions between activatable states, which include vacant and liganded states of both the open and closed channel. Figure 1 shows example clusters from cloned mouse $\alpha\beta\delta\gamma$ (embryonic-type) AChR expressed in HEK 293 cells exposed to either 10 μM ACh, 100 μM carbamylcholine (CCh), or 1000 μM tetramethylammonium (TMA). In these patches the mean probability of being open within a cluster (P_{open}) was, respectively, 0·46, 0·62 and 0·48. At lower agonist concentrations the rate of ligand binding is low, resulting in long closed times within clusters and low P_{open} values. At higher agonist concentrations the binding rates are high, resulting in short closed times and high P_{open} values.

A cluster-based analysis of the kinetics of activation is limited to a range of agonist concentrations. At the low end, when the P_{open} values become very small (less than ~0·1), clusters arising from a single channel are difficult to define. At the high end, channel block by agonist molecules lowers the amplitude and increases the variance of the single-channel current forcing low-pass filtering and a concomitant loss in the detection of short-lived events. Both the lower and upper limits vary with the agonist. For the three agonists that we have examined, the approximate useful ranges were 2–500 μM for ACh, 10–2000 μM for CCh, and 200–20 000 μM for TMA.

Dose–response curves

The dose–response curve is a simple measure of the activation reaction. Dose–response profiles for embryonic AChR expressed in HEK cells and activated by ACh, TMA and CCh are shown in Fig. 1. Our measured response, the cluster P_{open}, is not equivalent to currents observed in whole-cell experiments, where channel block and desensitization may influence the macroscopic current amplitude. In our analysis, P_{open} values were calculated from idealized records and did not depend on the amplitude of the open channel current; thus they reflect the probability that a channel will reside in an open state within the set of activatable (non-blocked and non-desensitized) states. Sojourns in the short-lived desensitized state are relatively rare and do not greatly influence the P_{open} estimate at intermediate agonist concentrations. At high agonist concentration, where such events would lower the cluster P_{open}, these sojourns were excluded.

For comparison with similar analyses in other laboratories, the P_{open} curves for each agonist were each fitted by the Hill equation:

$$P_{open} = P_{max}/(1 + (EC_{50}/A)^n), \quad (1)$$

where A is the agonist concentration, P_{max} is the maximum P_{open}, n is the Hill coefficient, and EC_{50} is the concentration producing a half-maximal response. The results of these fits are shown in Table 1. The most significant difference between the curves for the three agonists is that those for CCh and TMA are right-shifted (~3-fold and 100-fold, respectively) relative to that for ACh.

Dose–response curves are a composite measure of the channel activation reaction because all of the rate constants of the activation pathway – binding, gating, and other events – combine to determine its position and shape. The decomposition of the P_{open} curve into individual binding and gating rate constants requires a kinetic model.

The standard model of AChR activation

The standard kinetic scheme for AChR activation holds that a channel-opening conformational change follows the sequential binding of two agonist molecules ([A]):

$$C \underset{k_{-1}}{\overset{[A]k_{+1}}{\rightleftharpoons}} AC \underset{k_{-2}}{\overset{[A]k_{+2}}{\rightleftharpoons}} A_2C \underset{\alpha}{\overset{\beta}{\rightleftharpoons}} A_2O$$

Model 1

The first three states of the model represent vacant (C), monoliganded (AC), and doubly liganded (A_2C) closed complexes, and the fourth is an ion-permeable (open) complex (A_2O). This is the simplest model that accounts for the basic properties of channel activation. Throughout this paper the association rate constants will be reported in the units of per micromolar per second, and all other rate constants as per second.

Table1. Dose–response parameters for ACh-, CCh- and TMA-activated receptors (fitted to eqn (1))

	P_{max}	EC_{50}	n
ACh	0·996 ± 0·010	9·44 ± 0·39	1·57 ± 0·09
CCh	0·969 ± 0·015	30·8 ± 1·85	1·49 ± 0·12
TMA	0·886 ± 0·023	868·0 ± 61·6	1·97 ± 0·25

An alternative activation scheme is:

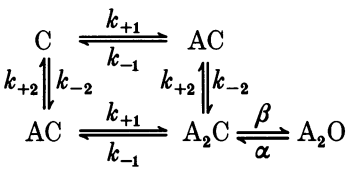

This model allows the random binding of agonists to two different but independent sites, whereas the linear scheme (model 1) forces sequential binding to two different sites. Although the random and sequential binding schemes have the same number of free parameters (6), they are distinct: random binding predicts that the closed interval probability density function (PDF) has four components while sequential binding predicts that there are only three. When the dissociation rate constants are very different, fitting to either class of model produces similar identical rate constant estimates (and LL values) because deactivation almost always proceeds by one pathway out of the A_2C state (Sine *et al.* 1990). With our rate constants, the extra closed interval component in the random binding scheme is very fast (< 50 μs) and constitutes a very small fraction of the total (< 0·1 %). This result indicates that the association and dissociation rate constants obtained by fitting the linear models are *single-site* rate constants, i.e. pertain to ACh binding to either of the two binding sites.

Properties of TMA-activated channels

Examples of clusters and of open and closed interval duration histograms at different TMA concentrations are shown in Fig. 2. TMA-activated channels have an open channel lifetime of 3·8 ± 0·9 ms ($n = 7$ patches; 5 kHz bandwidth; 0·2–10 mM TMA). The apparent opening rate (β'; see Methods for definition) increases with increasing concentrations of TMA and shows saturation at very high concentrations (Fig. 5, middle panel). When fitted to the Hill equation (eqn (1), with β_{max} replacing P_{max}) these data predict a maximum opening rate of 3148 ± 640 s^{-1}. According to model 1, this limit defines the intrinsic opening rate constant, β. The fitted value of β is within a factor of 2 of that reported by Mody, Lee & Dilger (1994), who estimate an opening rate constant of 1600 s^{-1} obtained by rapid perfusion of TMA to outside-out patches from mouse BC3H1 cells, which also express $\alpha\beta\delta\gamma$ AChR.

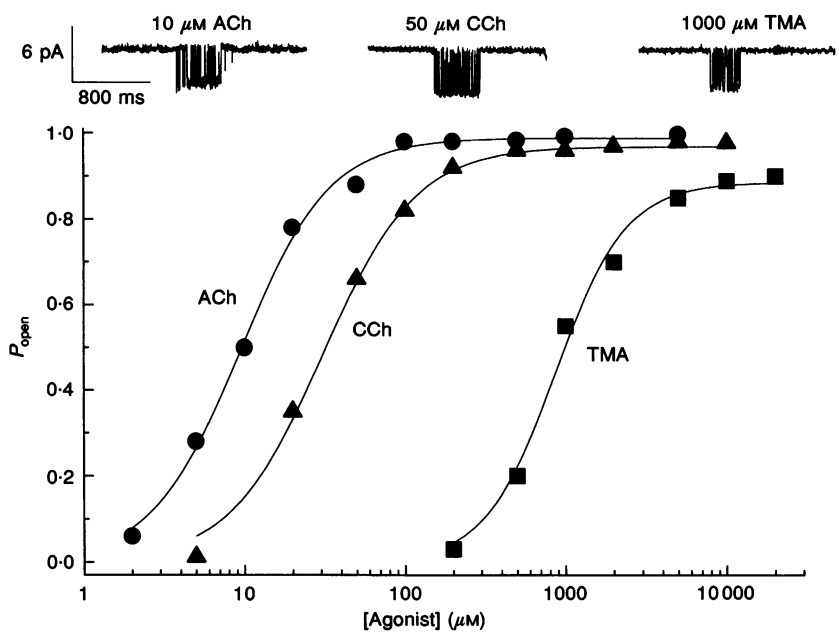

Figure 1. Single-channel records and dose–response curves of mouse AChR expressed in HEK cells

A, examples of clusters at low time resolution (higher resolution views are in Figs 2–4). *B*, the probability of being open within a cluster (P_{open}) is plotted as a function of the agonist concentration. The P_{open} was calculated from the idealized intervals within clusters using an equal number of open and closed interval durations. The symbols are means (1–6 patches at each concentration; 7–120 clusters in each patch) and the lines are drawn to the Hill equation, according to the parameters given in Table 1.

The closed interval duration histograms show a fast component of closures that do not vary substantially in either frequency or duration with the concentration of TMA. These gaps were of short duration (30 ± 23 μs; 7 patches) and although their frequency varied considerably from patch to patch, when present they were common (on average, they occurred about every 9 ms of open time). According to the standard interpretation (model 1), the lifetime of gaps associated with transitions between the A_2C and A_2O states are equal to $(k_{-2} + \beta) - 1$ and the frequency of these gaps (per open interval) is equal to (β / k_{-2}). However, this interpretation of the brief gaps is not

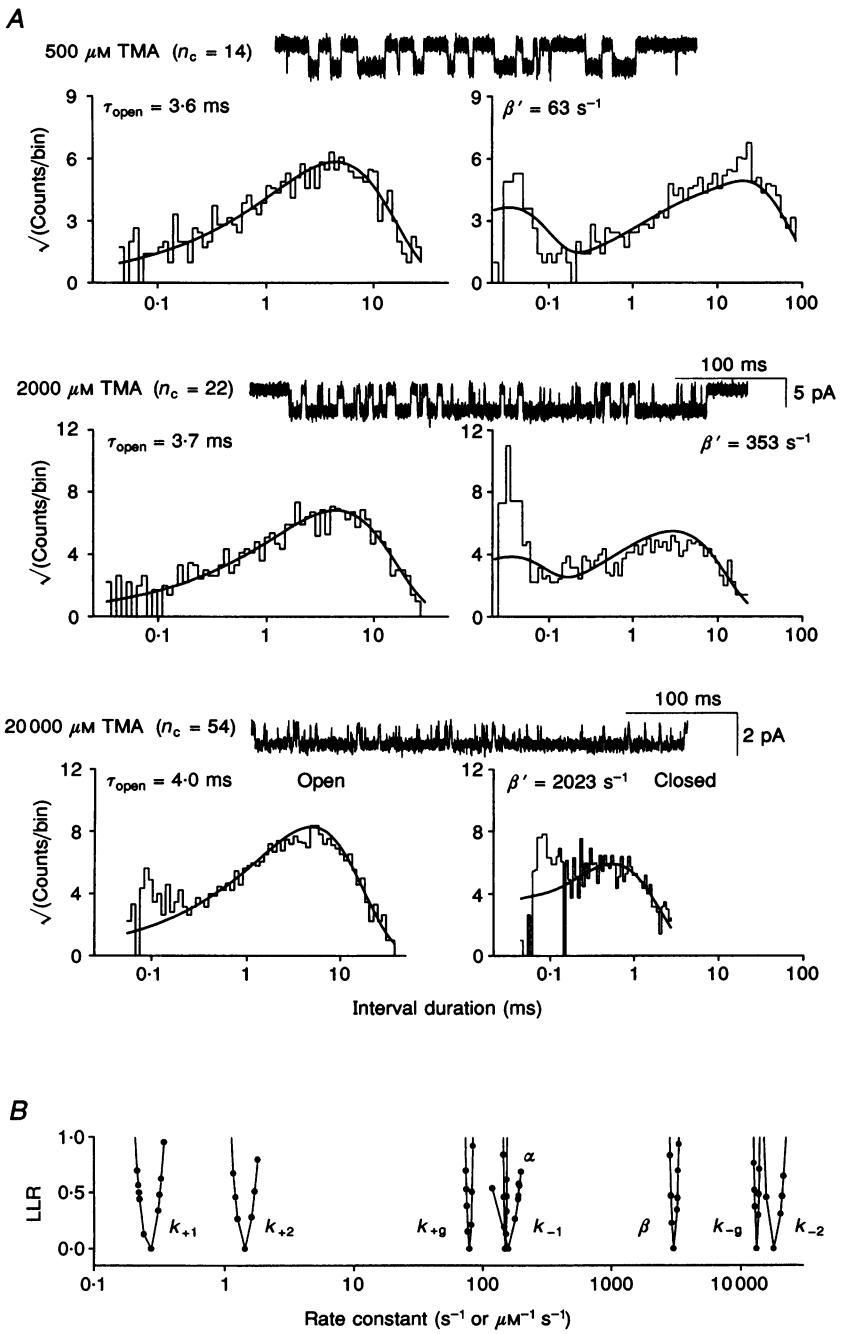

Figure 2. Kinetics of TMA-activated currents

A, examples of TMA-activated currents and open/closed interval duration histograms at several agonist concentrations. The binned data are from single patches (n_c, number of clusters) idealized with the Viterbi algorithm and the continuous lines are calculated directly from the overall rates obtained from many different patches (model 2; see Table 3 and text for the values) with no fitting of the binned data. The example cluster at 20 mM TMA has a reduced amplitude because of channel block. *B*, log likelihood surface in the region of the optimal rates (model 2). The parabolic shape indicates the rate constants were well defined, with S.E.M. equal to the width of each parabola at log likelihood ratio (LLR) = 0·5.

consistent with the observed saturation in β': brief and frequent gaps are not expected if the opening rate constant is slow (e.g. 3000 s^{-1} in TMA-activated receptors), in which case the gaps would be longer lived and, in particular, more infrequent than those that were observed. The ambiguities of associating brief gaps with a particular kinetic state have been pointed out by several groups (Auerbach & Sachs, 1983; Colquhoun & Sakmann, 1985; Sine & Steinbach, 1987).

This result suggests that not all of the brief gaps reflect the A_2C–A_2O gating transition. As codified by the following scheme, we propose that some brief gaps represent sojourns in another short-lived closed state (A_2C^*) that is not in the main activation pathway but that is connected to the open state:

$$C \underset{k_{-1}}{\overset{[A]k_{+1}}{\rightleftharpoons}} AC \underset{k_{-2}}{\overset{[A]k_{+2}}{\rightleftharpoons}} A_2C \underset{\alpha}{\overset{\beta}{\rightleftharpoons}} A_2O \underset{k_{-g}}{\overset{k_{+g}}{\rightleftharpoons}} A_2C^*$$

Model 2

where k_{+g} and k_{-g} are the rate constants of entry into and exit from this short-lived gap state. When model 2 was fitted to the TMA data set, the following rate constants produced the maximum likelihood (see Fig. 2*B*):

$$C \underset{158}{\overset{0{\cdot}3[TMA]}{\rightleftharpoons}} AC \underset{17\,923}{\overset{1{\cdot}4[TMA]}{\rightleftharpoons}} A_2C \underset{149}{\overset{3023}{\rightleftharpoons}} A_2O \underset{30\,132}{\overset{114}{\rightleftharpoons}} A_2C^*$$

(TMA rate constants)

This scheme adequately describes all of the available experimental results. The fitted opening rate constant (3023 ± 304 s^{-1}) is consistent with the value estimated from the saturation in the apparent opening rate (3148 ± 640 s^{-1}). The open and closed PDFs calculated directly from the rate constants (no fitting) describe the experimental interval duration histograms over a wide range of TMA concentrations (Fig. 2). In addition, the dose–response, binding and β' curves that we calculate directly from these rate constants (no fitting) superimpose on the experimental data over a 1000-fold range of TMA concentrations (Fig. 5). The above rate constants describe the steady-state currents, single-channel interval durations, opening kinetics and equilibrium binding.

The rate constants (model 2) predict that at low concentrations of TMA (and with a dead time of 25 μs) the component of brief gaps in the closed interval duration histograms should consist of two components, a 48 μs gap (18% of all brief gaps) that is associated with A_2C–A_2O gating with the remainder being a 33 μs gap that is associated with sojourns in A_2C^*. Colquhoun & Sakmann (1985) noted that at low concentrations of decamethonium, in the experiments with the highest analysis bandwidths the durations of brief gaps were distributed as the sum of two exponentials, a fact that indicates the existence of two short-lived closed states.

Equilibrium constants for the activation reaction can be calculated from the fitted rate constants. TMA binds to the first site with a K_{d1} of 526 μM, and to the second with K_{d2} of 12 802 μM. The first site is kinetically slower and has a 25 times higher affinity for TMA. Here, association is ~5 times slower and dissociation is >100 times slower than at the second site. The gating rate constants indicate that TMA opens channels rather effectively, with the gating equilibrium constant, Θ ($=\beta/\alpha$), equal to 20. Note, however, that the closing rate constant for TMA-activated receptors is likely to be an underestimate because at high concentrations of agonist the apparent open channel lifetime is prolonged because of unresolved channel block. Finally, the probability of residing in the A_2C^* state is low, with $K_g(k_{+g}/k_{-g}) = 0{\cdot}006$.

Characteristics of ACh-activated channels expressed in HEK cells

The properties of wild-type AChRs were studied in 47 cell-attached patches that were exposed to 1 μM–5 mM ACh (Table 2). Examples of clusters and of open and closed interval duration histograms are shown in Fig. 3.

Up to 500 μM ACh, the apparent opening rate increases to about 25 000 s^{-1}, with no clear saturation present (Fig. 5, middle panel). Above this concentration of ACh, the filtering necessitated by channel block made the identification and detection of the short closures unreliable (Fig. 3*A*, bottom panel). At all concentrations of ACh, a fast gap component was present, with a mean lifetime of $19{\cdot}3 \pm 10{\cdot}2$ μs ($n = 24$ patches, 1–50 μM ACh, HEK cells only). These results suggest that the intrinsic channel opening rate constant, β, with ACh as the agonist is >25 000 s^{-1}.

The lack of saturation in the apparent opening rate allows us only to set a lower limit on β. Maconochie & Steinbach (1992) report that upon very fast (<100 μs rise time) application of ACh (up to 10 mM) to outside-out patches, mouse embryonic channels expressed in a fibroblast cell line open at ~60 000 s^{-1}. Moreover, the rise time of the averaged currents to a step increase in ACh continues to decrease between 0·5 and 5 mM ACh, suggesting that there is a low affinity binding step. Several groups have reported such a low affinity binding process (Jackson, 1988; Sine *et al.* 1990).

According to model 1, the inverse lifetime of the briefest closed interval component (sojourns in A_2C) is equal to $\beta + k_{-2}$. If the opening rate constant is indeed this fast, then the duration of the brief gaps that we measure may not be consistent with their quantitative assignment as sojourns in A_2C. If, for example, $\beta > 60\,000$ s^{-1}, then the lifetime of the A_2C state would be <16 μs. The lifetime of this state is certainly shorter still, because dissociation also terminates sojourns in A_2C. For example, if k_{-2} were 40 000 s^{-1}, the mean lifetime of the A_2C state would be <10 μs. These durations are near or below our detection limit and suggest that the ~19 μs gaps that we observe in the records at all ACh concentrations cannot be reliably

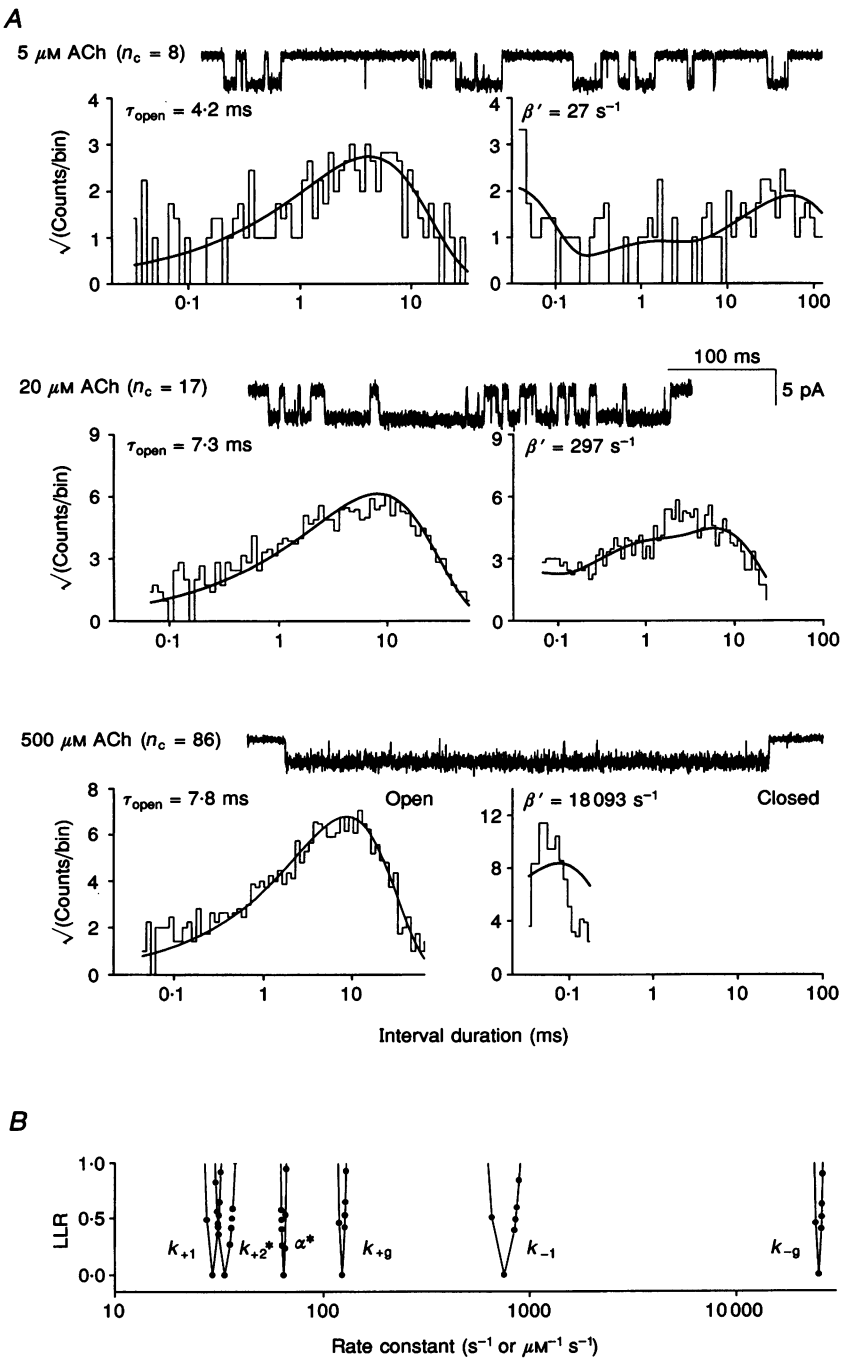

Figure 3. Kinetics of ACh-activated currents

A, examples of ACh-activated currents and open and closed interval duration histograms at several agonist concentrations. The binned data are from single patches (n_c, number of clusters) idealized with the Viterbi algorithm and the continuous lines are calculated directly from the overall rates obtained from many different patches (model 2; see Table 3 and text for the values); k_{+g} and k_{-g} were fitted independently for each file. The 20 μM file is from AChR expressed in oocytes. *B*, log likelihood surface in the region of the optimal rates (model 3), expressed as log likelihood ratios (LLR) relative to the optimal fit. The parabolic shape indicates the rate constants were well defined, with S.E.M. equal to the width of each parabola at LLR = 0·5.

Table 2. Average rates for ACh-activated receptors

Model 3

	k_{+1} (μM^{-1} s^{-1})	k_{-1} (s^{-1})	k_{+2}* (μM^{-1} s^{-1})	α* (s^{-1})	k_{+g} (s^{-1})	k_{-g} (s^{-1})
Oocytes (n =8)	43	931	87	95	375	34162
HEK cells (n =26)	15	1451	78	68	57	25649
HEK and oocytes (n =34)	37 ± 24	1053 ± 933	85 ± 61	88 ± 68	300 ± 209	35347 ± 23467

Model 1

	k_{+1} (μM^{-1} s^{-1})	k_{-1} (s^{-1})	k_{+2} (μM^{-1} s^{-1})	k_{-2} (s^{-1})	β (s^{-1})	α (s^{-1})
Oocytes (n =8)	23	1748	85	5526	25000†	253
HEK cells (n =26)	44	1085	93	5687	27790	413
HEK and oocytes (n =34)	39 ± 30	1241 ± 791	91 ± 64	5649 ± 2488	27135 ± 12761	376 ± 204

Except where noted, all six rate constants of the activation scheme were independently estimated for each patch. The concentration range was 2–100 μM. †β was fixed at this value. Values for HEK cells and oocytes are means ± S.D.

used to estimate $\beta + k_{-2}$. We speculate that our estimates of the gap durations are longer than the true values because of limited resolution, and/or that ACh-activated receptors, like those activated by TMA, can enter a short-lived closed state that is connected to the open state but that is not in the main activation pathway.

A modified activation model

If the opening rate constant is 60000 s^{-1}, model 2, which is the full description of the events within clusters, cannot be used to fit the ACh single-channel data because the A_2C state would be too brief to be reliably detected. Moreover, we could not distinguish those gaps that reflect sojourns in A_2C from those that reflect sojourns in A_2C^*. We therefore imposed the condition that in our experiments all of the brief gaps arise from A_2O–A_2C^* transitions, i.e. that all of the A_2C–A_2O transitions are missed. Accordingly, model 2 must be modified to incorporate an undetectably short dwell time in A_2C. This is accomplished simply by deleting A_2C and directly connecting the AC and A_2O states:

$$C \underset{k_{-1}}{\overset{[A]k_{+1}}{\rightleftharpoons}} AC \underset{\alpha^*}{\overset{[A]k_{+2}^*}{\rightleftharpoons}} A_2O \underset{k_{-g}}{\overset{k_{+g}}{\rightleftharpoons}} A_2C^*$$

Model 3

where k_{+2}* and α* are *apparent* association and closing rate constants, respectively.

We can compare the rate constants obtained from fitting to model 3 with those obtained by the use of model 1 or model 2. Information is lost by the elimination of A_2C gaps from the analysis; the rate constants of the AC–A_2O step of model 3 are composite in that they convolve binding and gating. If the durations of sojourns in the 'missed' state are vanishingly small, then the rate constants according to model 3 bear a simple relationship with those of model 1:

$$\begin{aligned} \alpha^*/k_{+2}^* &= K_{d2}/\Theta, \\ k_{+2} &= k_{+2}^*/\Phi, \\ \alpha &= \alpha^*/(1-\Phi), \\ \Phi &= \beta/(\beta + k_{-2}), \end{aligned} \qquad (2)$$

where Φ defines the fraction of fully occupied receptors that open.

Sojourns in the A_2C state, while not directly detectable as gaps, are manifest as a slowing of the apparent association and dissociation rate constants relative to the actual rate constants. Intuitively, some of the transitions out of AC (or A_2O) are 'unproductive' because the system instantaneously returns to the starting state. The value of Φ (or $1 - \Phi$) gives the fraction of transitions that are unproductive. With TMA, the fit to model 2 indicates that this Φ is 0·14.

Activation rate constants of ACh-activated channels expressed in HEK cells

Each of thirty-four patches (1–100 μM ACh) was separately fitted to either model 1 or model 3. The average rate constants are shown in Table 2. In any given patch, the LL values were identical for the two kinetic schemes; Keinker (1989) has shown that CCCO and CCOC models are indistinguishable in the steady state; thus we cannot use the LL values to compare model suitability.

To estimate activation rate constants for ACh we selected clusters from several patches from the steep region of the dose–response curve (5–20 μM ACh) that had P_{open} values that were within 0·05 units of the means. The idealized currents from these ten patches (12884 intervals;

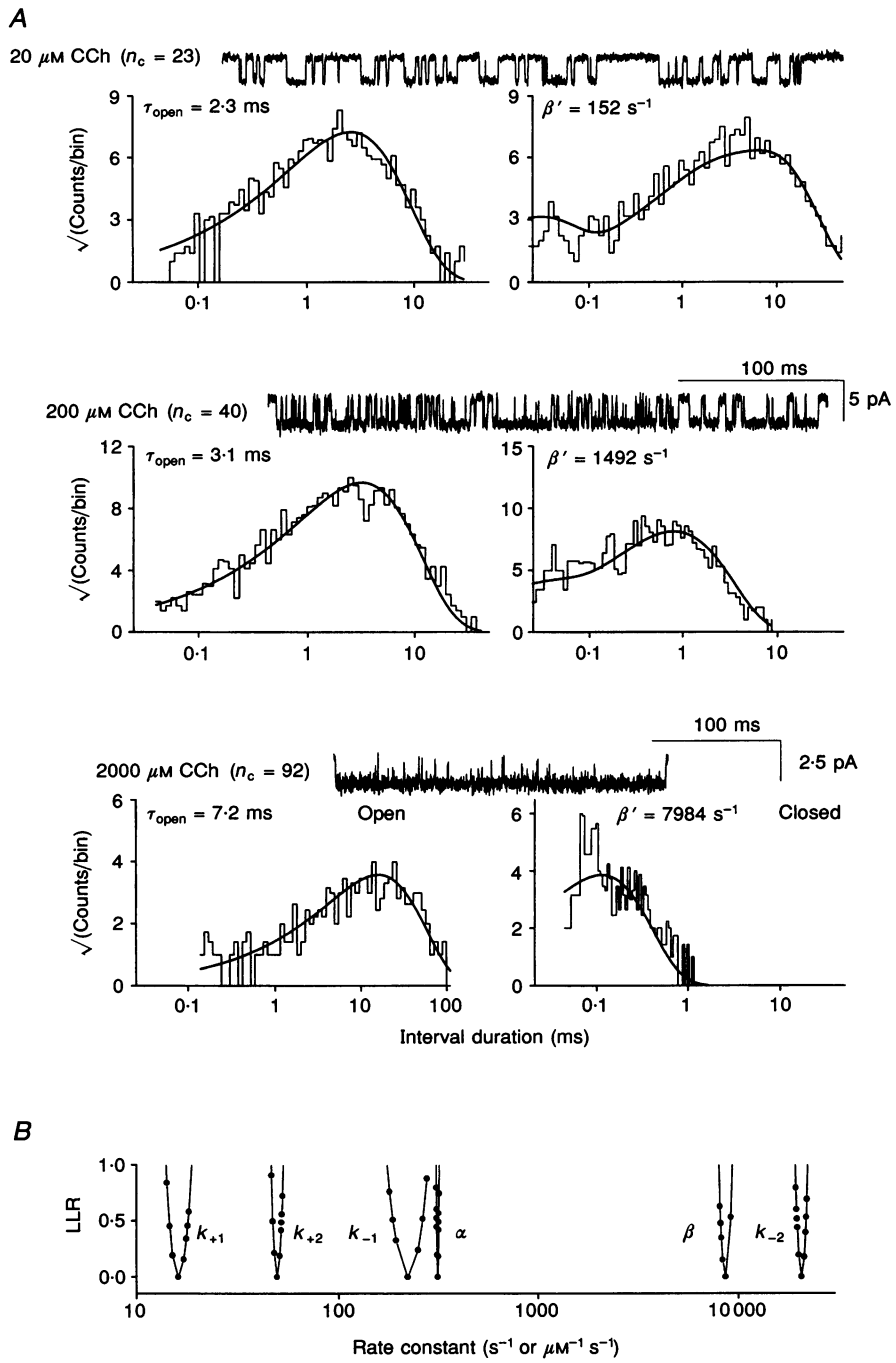

Figure 4. Kinetics of CCh-activated currents

A, examples of CCh-activated currents, and open and closed interval duration histograms at several agonist concentrations. The binned data are from single patches (n_c, number of clusters) idealized with the Viterbi algorithm and the continuous lines are calculated directly from the overall rates obtained from many different patches (model 2; see Table 3 and text for the values) with no fitting of the binned data. The example cluster at 2 mM CCh has a reduced amplitude because of channel block. *B*, log likelihood surface in the region of the optimal rates (model 1). The parabolic shape indicates the rate constants were well defined, with S.E.M. equal to the width of each parabola at LLR = 0·5.

128 clusters) were fitted together to get activation rate constant estimates and their S.E.M. The fitted rate constants were (see Fig. 3*B*):

$$C \underset{616}{\overset{31[ACh]}{\rightleftharpoons}} AC \underset{8205}{\overset{48[ACh]}{\rightleftharpoons}} A_2C \underset{186}{\overset{14\,455}{\rightleftharpoons}} A_2O$$

(ACh, model 1)

$$C \underset{616}{\overset{29[ACh]}{\rightleftharpoons}} AC \underset{73}{\overset{28[ACh]}{\rightleftharpoons}} A_2O \underset{24\,866}{\overset{122}{\rightleftharpoons}} A_2C^*$$

(ACh, model 3)

For both kinetic schemes, the rate constants were well defined and could adequately describe the dose–response, binding, and apparent opening rate curves.

According to either model, the equilibrium binding constant of ACh at the first site, K_{d1}, is ~20 μM, and the association rate constant of the second site is faster than at the first (recall that with model 3 the observed rate constant k_{+2}^* always underestimates the actual rate constant k_{+2}). The two schemes differ in their predictions about the opening rate constant. Fitting to model 1 yields an opening rate constant of ~15 000 s^{-1}, while fitting to model 3 accommodates an arbitrarily fast opening rate constant. Similarly, fitting to model 1 results in a K_{d2} of 171 μM, while fitting to model 3 accommodates an arbitrarily low affinity at the second site.

Four rate constants of model 1 (k_{+2}, k_{-2}, β and α) are compressed into two in model 3 (k_{+2}^* and α^*); thus two additional free parameters are needed if we are to estimate the equilibrium binding affinity to the second site. First, we will assume that the opening rate constant is 60 000 s^{-1} (Maconochie & Steinbach, 1992). Another parameter that constrains the rate constant estimates is the high concentration limit of the ACh dose–response curve (0·996; Fig. 1). This value was obtained by fitting the results of experiments at concentrations that were outside the range used in the single-channel analyses, up to 5 mM ACh. Combining these measures with the fits of model 3 to the single-channel currents we calculate using eqn (2) the following rate constants for activation by ACh:

$$C \underset{616}{\overset{29[ACh]}{\rightleftharpoons}} AC \underset{27\,000}{\overset{40[ACh]}{\rightleftharpoons}} A_2C \underset{240}{\overset{60\,000}{\rightleftharpoons}} A_2O$$

(ACh rate constants)

The error limits on these rate constants are large because the fitted value for the maximum P_{open} is close to unity. However, we think that the maximum P_{open} estimate is a lower limit because sojourns in the A_2C^* will lower the apparent P_{open}. For these reasons the rate constants and equilibrium constants should be expressed as limits rather than as absolute values: $\alpha < 240\ s^{-1}$, $k_{+2} > 40\ \mu M^{-1}\ s^{-1}$, $k_{-2} > 27\,000\ s^{-1}$, $\Theta > 250$, $\Phi < 0{\cdot}7$ and $K_{d2} > 675\ \mu$M. All values of rate constants that are within these limits can account for the single-channel properties.

The ability of these rate constants to describe the experimental data is shown in Figs 3 and 5. Model 2 was used to compute the PDFs, with the above activation rate constants; the rate constants k_{+g} and k_{-g} were fitted independently for each file. Dose–response, effective opening rate, and equilibrium binding curves were also calculated directly from these parameters. As was the case with TMA, the rate constants account for the experimental results.

The effects of different expression systems

The P_{open} dose–response curve values for embryonic receptors expressed in oocytes only were fitted by eqn (1) with these results: $P_{max} = 0{\cdot}99$, $EC_{50} = 11\ \mu$M, $n = 1{\cdot}5$. These values are similar to that obtained by fitting the HEK cell dose–response curve, and are in excellent agreement with the values from dose–response profiles obtained from perfusion (< 0·1 s rise time) of ACh to excised outside-out patches from oocytes injected with mouse BC3H1 AChR subunits (Tomaselli, McLaughlin, Jurman, Hawrot & Yellen, 1991). The agreement suggests (1) that the activation properties of AChR expressed in oocytes and HEK cells are similar, (2) that excision does not substantially alter channel dose–response properties, and (3) that channels that become active after having desensitized behave similarly to those that have never desensitized.

For the single-channel kinetic analyses, the oocyte and HEK cell receptors were treated as different populations and the activation rate constants were estimated from the average values computed on a file-by-file basis for each population. The results (Table 1) indicate that the average binding and gating rate constants of receptors expressed in oocytes or HEK 293 cells are similar. Because the standard deviations of the rate constants were large we cannot be sure that the lower affinity of the first binding site in AChR expressed in oocytes is significant. The biggest difference between the two populations was that k_{+g} was much smaller in oocyte-expressed receptors, a fact that can be readily attributed to the lower analysis bandwidth in the oocyte experiments (see Methods).

Activation rate constants of CCh-activated channels expressed in HEK cells

The properties of wild-type AChR were studied in thirteen cell-attached patches exposed to 5–10 000 μM CCh. Examples of clusters and of open and closed interval duration histograms at different CCh concentrations are shown in Fig. 4. CCh-activated channels have an open channel lifetime of 3·30 ± 0·7 ms ($n = 6$ patches; 3 kHz bandwidth).

The effective opening rate shows saturation at high CCh concentrations (Fig. 5). When fitted by eqn (1), these data indicate that $\beta_{max} = 11\,045 \pm 986\ s^{-1}$. To estimate activation rate constants, intervals from six patches (16 040 intervals, 210 clusters) were fitted by either models 1 or 3 (see Fig. 4*B*):

$$C \underset{163}{\overset{14[CCh]}{\rightleftharpoons}} AC \underset{20544}{\overset{49[CCh]}{\rightleftharpoons}} A_2C \underset{312}{\overset{8619}{\rightleftharpoons}} A_2O$$

(model 1, CCh rate constants)

$$C \underset{212}{\overset{16[CCh]}{\rightleftharpoons}} AC \underset{239}{\overset{13[CCh]}{\rightleftharpoons}} A_2O \underset{20635}{\overset{61}{\rightleftharpoons}} A_2C^*$$

(model 3, CCh rate constants)

The rate constants with either model were well defined and describe the dose–response, apparent opening rate, and binding curves as well as the single-channel open and closed duration histograms. According to model 1 $K_{d1} = 12\ \mu M$, $K_{d2} = 420\ \mu M$, $\Theta = 28$ and $\Phi = 0{\cdot}30$. We attempted to fit the CCh data to model 2 in the hope that

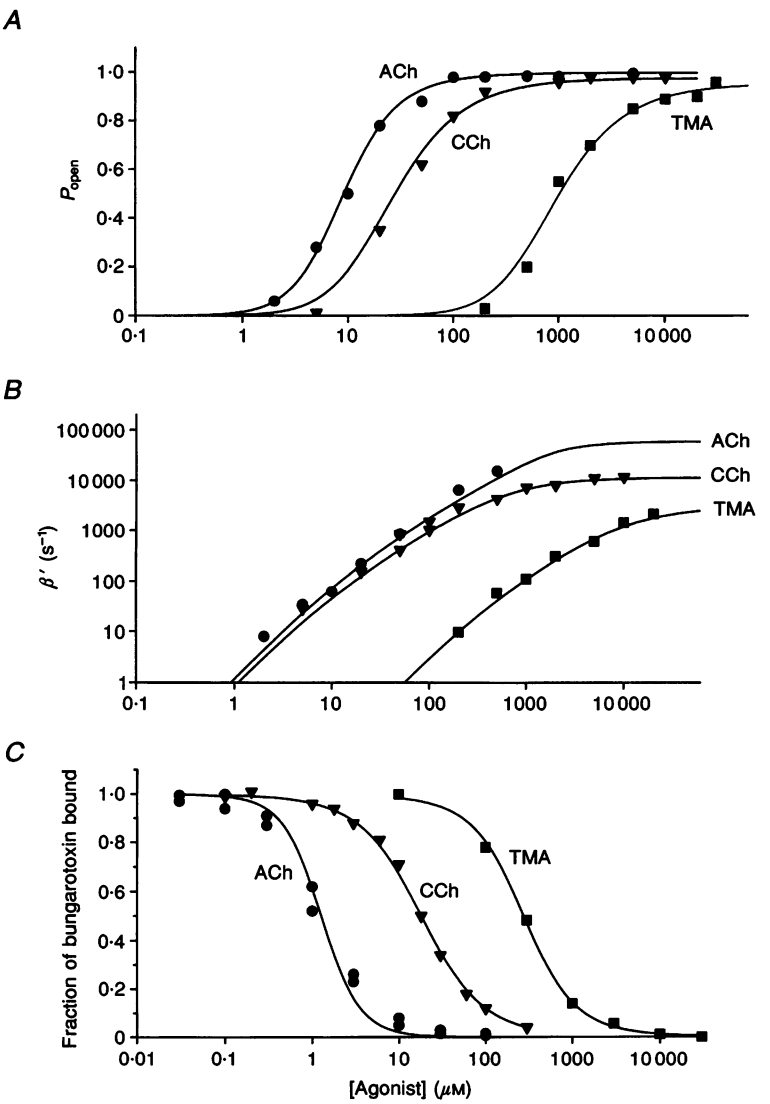

Figure 5. Observed and predicted activation properties of AChR activated by ACh, CCh, or TMA

A, dose–response curves; *B*, effective opening rates (β'); *C*, equilibrium binding curves. For the dose–response and effective opening rate data, the continuous lines are calculated from the rates (model 1; see Table 3) without curve fitting and the symbols are experimental observations. The equilibrium binding curve (bungarotoxin competition, 0 mV membrane potential) experimental data are from Sine *et al.* (1994); the continuous lines are drawn according to the rates given the Table 3 (Θ values were divided by 10 to reflect the depolarized membrane potential) plus one fixed parameter (the equilibrium constant for the desensitization of vacant channels) and one fitted parameter (the equilibrium binding constant to the desensitized receptor).

Table 3. Binding and gating parameters for TMA-, ACh- and CCh-activated receptors

	k_{+1} (μM^{-1} s^{-1})	k_{-1} (s^{-1})	k_{+2} (μM^{-1} s^{-1})	k_{-2} (s^{-1})	β (s^{-1})	α (s^{-1})	K_{d1} (μM)	K_{d2} (μM)	Θ
TMA	0·31	158	1·4	17920	3023	>150	526	12802	20
ACh	29	616	>40	>27000	60000*	<240	21	>675	>250
CCh	16	221	40	22830	11450	359	14	571	32
	k_{+1}	k_{-1}	k_{+2}	k_{-2}	β	α	K_{d1}	K_{d2}	Θ
ACh/TMA	94	3·9	>29	>1·5	20	<1·6	0·040	>0·053	>12
CCh/TMA	52	1·4	29	1·3	3·8	2·4	0·027	0·045	1·6
	k_{+1}	k_{-1}	k_{+2}	k_{-2}	β	α	K_{d1}	K_{d2}	Θ
ACh/TMA ΔΔG (kcal mol^{-1})	2·7	0·8	2·0	0·2	1·8	0·3	−1·9	>−1·7	>1·5
CCh/TMA ΔΔG (kcal mol^{-1})	2·3	0·2	2·0	0·1	0·8	0·5	−2·1	−1·8	0·3

The relative values are the ratio $\text{rate}_{\text{ACh or CCh}}/\text{rate}_{\text{TMA}}$. These results are shown in graphical form in Fig. 6.
* From Maconochie & Steinbach (1992).

the modelling would detect gap components that could be associated with both the A_2C and A_2C^* states. These attempts were unsuccessful.

With CCh, the results obtained by single-channel modelling and from the saturation in the dose–response curve agree. We nonetheless applied the same analysis methods as with ACh to extract the CCh activation rate constants (the rate constants of model 3, $\beta = 11450$ s^{-1}, $P_{max} = 0{\cdot}963$):

$$C \underset{212}{\overset{15[CCh]}{\rightleftharpoons}} AC \underset{22830}{\overset{40[CCh]}{\rightleftharpoons}} A_2C \underset{360}{\overset{11450}{\rightleftharpoons}} A_2O$$

(CCh rate constants)

From these values we estimate equilibrium binding constants of 14 and 570 μM at the two binding sites, respectively. As with the other agonists, association and dissociation at the first site is slower than to the second. The gating equilibrium constant, Θ, is 32, and the opening efficacy, Φ, is 0·33.

Comparison of model and experimental results

Figure 5 shows a comparison of the experimental observations with those that of model 1 according to the rate constants given in Table 3. The dose–response curves for all three agonists, shown in the top panel, are well described by the rate constants. The effective opening rate (β'), shown in the centre panel, is also well accounted for over about a 100-fold range of agonist concentration. We emphasize that the continuous lines in the top and centre panels of Fig. 5 are not curve fits to the experimental points, but rather are calculated directly from the rate constant estimates obtained from log likelihood fitting of the idealized single-channel currents. In the bottom panel, equilibrium binding results are replotted from Sine *et al.* 1994. Only one parameter, K_r, was fitted to the experimental data (see Methods). To take into account the fact that our activation rate constants were obtained at −90 mV while the binding experiments were at 0 mV, we reduced the Θ values 10-fold: an e-fold increase in α with a 40 mV depolarization (and no voltage dependence of β) would alter Θ by this factor. The continuous lines in the right panel of Fig. 5 were drawn to the fitted estimates $K_{r,ACh} = 13 \pm 0{\cdot}8$ nM, $K_{r,CCh} = 200 \pm 6{\cdot}8$ nM and $K_{r,TMA} = 2{\cdot}8 \pm 0{\cdot}2$ μM. These are in good agreement with the experimentally obtained values $K_{r,ACh} = 17$ nM, $K_{r,CCh} = 200$ nM (Sine *et al.* 1994) and $K_{r,TMA} = 1{\cdot}7$ μM (S. M. Sine, personal communication). Thus, both equilibrium and kinetic aspects of binding and activation are described by the rate constants given in Table 3.

Activation rates according to other models

The idealized currents were fitted to a scheme in which each ligand binding event is followed by a kinetically resolvable state change. Such a random sequential, or stepwise, model has been applied to both *Xenopus* myocyte (Auerbach, 1993) and cloned mouse (Auerbach, 1992) AChR kinetics. A related scheme has been used to describe the gating of *Shaker* K channels (Zagotta, Hoshi & Aldrich, 1994). In the stepwise scheme, C is a resting receptor, C′ is a receptor that has undergone one state change (but is still non-conducting), and O is a receptor than has undergone two state changes and is open:

$$C \underset{k_{-1}}{\overset{[A]k_{+1}}{\rightleftharpoons}} AC \underset{\alpha}{\overset{\beta}{\rightleftharpoons}} AC' \underset{\alpha^*}{\overset{[A]k_{+2}^*}{\rightleftharpoons}} A_2O \underset{k_{-g}}{\overset{k_{+g}}{\rightleftharpoons}} A_2C^*,$$

Model 4

where β and α are the forward and reverse isomerization rates for the monoliganded receptor, and all other rates are as in model 3.

Idealized currents from eight patches (12 884 intervals, 219 clusters, 1–200 μM ACh, $\tau_{dead} = 25$ μs) were fitted by either model 3 (concerted) or model 4 (stepwise). The optimal rates were:

$$C \underset{773}{\overset{25[ACh]}{\rightleftharpoons}} AC \underset{66}{\overset{72[ACh]}{\rightleftharpoons}} A_2O \underset{25\,866}{\overset{253}{\rightleftharpoons}} A_2C^*$$

(model 3)

$$C \underset{710}{\overset{34[ACh]}{\rightleftharpoons}} AC \underset{3203}{\overset{2396}{\rightleftharpoons}} AC' \underset{67}{\overset{101[ACh]}{\rightleftharpoons}} A_2O \underset{25\,040}{\overset{249}{\rightleftharpoons}} A_2C^*$$

(model 4)

The log likelihood surfaces in the vicinity of the optimal rates were parabolic, i.e. all of the parameters were well defined. The stepwise model (8 rate constants, LL = 70 446) fitted the interval durations better than did the concerted model (6 rate constants, LL = 70 343). The magnitude of the log likelihood ratio (LLR) for this comparison, 103, indicates that the better fit is more than would be expected solely from the addition of two extra free parameters (Horn, 1987).

One interpretation of the AC–AC′ transition is that it reflects a structural change in a monoliganded receptor that is analogous with the opening of doubly liganded receptors (Auerbach, 1993). The optimal rate constants for this transition for monoliganded receptors (β and α) are, respectively, ~25 times slower and ~15 times faster than the equivalent rate constants for doubly liganded receptors, β and α. This means that the equilibrium constant for the monoliganded conformational step (β/α) is about 375 times smaller ($\Delta\Delta G_o = 3{\cdot}5$ kcal mol^{-1}) than that of the doubly liganded step (β/α).

We also fitted the intervals to models that had a monoliganded open state, connected either to AC (concerted model) or to AC′ (stepwise model). In the stepwise scheme, a monoliganded opening could occur when one gating domain has bound ligand and undergone a conformational change while the other, unliganded gating domain opens spontaneously. The results of fitting to either model were similar: the opening rate constant for monoliganded receptors was 210 ± 22 s^{-1} and the closing rate constant of monoliganded receptors was $12\,500 \pm 890$ s^{-1}. Compared with models 3 and 4, the addition of a monoliganded open state (and two additional free parameters) greatly improved the fit (LLR = 702 and 650 for concerted and stepwise models, respectively).

If we assume that all brief openings reflect the full allosteric opening transition of a monoliganded receptor, these results indicate that the opening rate constant is ~300 times slower and the closing rate constant is ~50 times faster when one of the binding sites is empty, or that the equilibirum constant for opening of monoliganded receptors is ~$1{\cdot}5 \times 10^4$ times smaller ($\Delta\Delta G_o = 5{\cdot}7$ kcal mol^{-1}) than that of doubly liganded receptors. This value is similar to that reported by Jackson (1988; $1{\cdot}2 \times 10^4$) for CCh-activated AChR in neonatal mouse muscle.

We emphasize that with these extended models, the association, dissociation, and opening and closing rate constant estimates were not significantly different from those obtained with the simpler activation schemes (models 1 and 3).

DISCUSSION

Models of receptor activation

To be successful, a quantitative kinetic analysis of activation should account for all of the relevant experimentally observed properties of the receptor. With AChR these include: (1) the shape and position of the dose–response curve, (2) the apparent affinities of ligand binding (as determined by competition with bungarotoxin), (3) the characteristics of the open and closed single-channel interval duration histograms over a wide range of agonist concentration, and (4) the rate of channel opening determined from the response to a step increase in the concentration of agonist and/or the saturation in the effective opening rate. Many of these features, for example the dose–response and binding curves, are in themselves poor guides for model discrimination as they can be readily fitted by a multitude of models and rate constants. Describing all of the experimental observations together, however, requires more constrained models and rate constants.

We were able to make such a global accounting (Fig. 5), and to estimate the rate constants of agonist association and dissociation, and channel opening and closing, only after making the following modifications to the basic CCCO activation model (model 1). First, we propose that some of the brief gaps that are apparent in the current records (and the closed duration histograms) represent transitions to a closed state that can only be reached after opening. This proposition adds an extra state to the basic kinetic scheme, which becomes CCCOC (model 2). Next, we suppose that with some agonists (e.g. ACh) the opening rate constant is very fast and our limited bandwidth does not allow us to detect accurately short-lived sojourns in the final closed step before opening. This allows us to remove this state from the scheme, which becomes CCOC (model 3).

The suitability of model 2 is supported by the fact that it can be used to account for all of the available data for ACh-, TMA- and CCh-activated channels: the dose–response curves, the agonist binding profiles, the differences in the binding properties of the two agonist binding sites, the single-channel interval histograms, and the opening rate to step change in agonist concentration. While model 1 can account for some of the above observations, it does not

account for the opening rate constants (as determined from concentration jumps) of TMA- and ACh-activated channels, or the apparently low affinity of the second binding site. We have not addressed the physical significance of the A_2C^* state which was particularly prevalent in TMA-activated receptors. *Shaker* K channels also enter a state that may be analogous to A_2C^*, i.e. a short-lived closed state that is connected to the main open state and that is not in the activation pathway (Hoshi, Zagotta & Aldrich, 1994).

Assignment of rate constants with binding sites

The rate constants of association and dissociation reflect the properties of either of the two binding sites. Unwin's (1993) structural analysis of the *Torpedo* AChR suggests that the binding sites each lie within an a subunit, and there is general agreement that the binding site properties are determined by α–δ and α–γ subunit pairs (Blount & Merlie, 1989; Pedersen & Cohen, 1990; Sine & Claudio, 1991).

We can attempt to associate the kinetic parameters, for example k_{+1} and k_{-1}, with either the $\alpha(\gamma)$- or $\alpha(\delta)$-sites of the receptor. Our rate constants indicate that the equilibrium dissociation constant of the first site is perhaps 25 times lower than that of the second site. Sine & Claudio (1991) have shown that CCh binds to non-desensitized mouse AChR (expressed in HEK cells) composed of only $\alpha\beta\delta$ with a K_d that is 10–100 times lower than those composed of only $\alpha\beta\gamma$-subunits. This result suggests that the first and second sites correspond to $\alpha(\delta)$ and $\alpha(\gamma)$, respectively. An observation that supports this hypothesis is that mutations in the δ-subunit at position W57Y influence the values of k_{+1} and k_{-1} but do not change k_{+2} and k_{-2} (Zhang, Chen & Auerbach, 1994). This δ-residue is affinity labelled by curare placing near a binding site, i.e. near α, which is consistent with our assignment of the first kinetic site to $\alpha(\delta)$.

Activation by ACh

The results of the single-channel kinetic modelling do not allow us to solve explicitly for all of the activation rate constants because model 3 can accommodate arbitrary values of β and k_{-2}. However, by combining the single-channel kinetic analyses with information about the saturation in the dose–response curve (Fig. 1) and the opening rate constant (which was too fast to be estimated from our single-channel data but has been measured by Maconochie & Steinbach (1992) we are able to set limits on the rate constants. The results indicate that the equilibrium binding constant of ACh to the $\alpha(\delta)$-site is $\sim$20 μM, the equilibrium binding constant of ACh to the $\alpha(\gamma)$-site is $>$650 mM, and the equilibrium binding constant for gating $>$250. ACh binds at least 25 times more tightly to the $\alpha(\delta)$-site than it does to the $\alpha(\gamma)$-site, mostly because of a slower rate constant of escape. Thus the $\alpha(\delta)$-site can be considered to be a high affinity, kinetically slow binding site. These results are very similar to those of Sine *et al.* (1990), who studied recombinant *Torpedo* AChR expressed in a fibroblast cell line.

Given the limits of our analysis, we can only state that the closing rate constant of ACh-activated channels is $<240\ s^{-1}$. Thus we can consider the interesting scenario that ACh- and TMA-activated channels close at the same rate, i.e. $150\ s^{-1}$. If we assume that this is true (and that $\beta = 60\,000\ s^{-1}$) then we arrive at a different set of rate constants for ACh activation that is also consistent with our single-channel data: $k_{+2} = 52\ \mu M^{-1}\ s^{-1}$, $k_{-2} = 51\,000\ s^{-1}$, $\Theta = 400$, $\Phi = 0{\cdot}54$ and $K_{d2} = 981\ \mu$M. The parameters associated with the first binding step do not change, so according to this interpretation, there would be a 46-fold difference in binding affinity between the two sites. Note that the closing rate constant for TMA-activated receptors is greater than $150\ s^{-1}$, because in our experiments at high agonist concentrations unresolved channel block by TMA prolonged the apparent open channel lifetime.

With regard to the gating step, the equilibrium probability of being open at very high ACh concentrations is, functionally, unity. However, the rate constants predict that in response to a transient pulse of ACh, as might be expected at a synapse, less than 70% the channels that become fully occupied actually open ($\Phi < 0{\cdot}7$) because ACh escapes from the $\alpha(\gamma)$-site before gating takes place.

The $>$25-fold higher affinity for ACh at the $\alpha(\delta)$-site can be attributed to a $>$50-fold slower dissociation rate constant at this site compared with the $\alpha(\gamma)$-site. The structural basis for this difference is unclear. The putative $\alpha(\delta)$-binding site appears to have a more sterically restricted entrance than does that in $\alpha(\gamma)$ (Unwin, 1993), but the markedly slower entry of TMA compared to ACh (see below) suggests that for TMA, diffusional or steric forces do not limit the association rate constant. Nonetheless, the two α-subunits have the same primary sequence and it is certain that residues from the neighbouring subunits influence both the rate of entry and, in particular, escape of ACh from the agonist binding sites, either by shaping the binding pocket and/or via making direct contacts with the ligand (Czajkowski, Kaufmann & Karlin, 1993).

Activation by different agonists

We can compare the activation of AChR by TMA, CCh and ACh by comparing the relative rate constants of each reaction step. This comparison is shown in Table 3 and Fig. 6. For the overall equilibrium of the activation reaction (C to A_2O), TMA-activated receptors require 5·3 kcal mol^{-1} more energy and CCh-activated receptors require 0·85 kcal mol^{-1} more energy compared with ACh-activated receptors.

The most striking difference between agonists is in their relative rate constants of association. TMA binds $\sim$100 times more slowly to the $\alpha(\delta)$-site, and $\sim$30 times more slowly to the $\alpha(\gamma)$-site, compared with ACh. In terms of relative free

energies, the association of TMA with the two sites requires 4·7 kcal mol^{-1} more energy than the association of ACh. The CCh binding rate constants, however, are similar to those of ACh. The slow binding of TMA (~10^5 M^{-1} s^{-1}) is well below the diffusional limit and is remarkable because TMA is smaller than both CCh and ACh and would thus be expected have a larger diffusion constant and to experience less steric restrictions upon binding. Our data indicate that diffusion or steric effects do not limit the rate of TMA binding, and that more subtle interactions of the agonist with the protein determine the association rate constant.

The proposition that the relative difference in the association rate constant between TMA and ACh arises from specific interactions of the ligand with the protein implies that an agonist molecule experiences one or more energy barriers/wells as it moves from solution to the docking site. In this sense, the binding of an agonist to a receptor might resemble ionic permeation: the energy of interaction of the agonist with the receptor protein (perhaps over a distributed structure) determines both the net 'flux' and 'selectivity' properties of the association reaction. We may speculate that the ability to select agonists based on these interaction energies (rather than simply by their concentrations) allows the receptor to exclude inorganic ions and metabolites from the docking site. The nature of the agonist–receptor interaction that allows rapid association is not known, but our data suggest that an esteratic group, or such a group in conjunction with a quaternary amine, imparts rapid binding. It is also possible the passage of the ligand from the solution to the docking site involves protein motions, as is the case for oxygen binding to haemoglobin (Case & Karplus, 1979), a protein that must exclude water from the docking site.

The relative dissociation rate constants for TMA, CCh and ACh are similar at both the $\alpha(\delta)$- and the $\alpha(\gamma)$-sites. The rate limiting steps to dissociation may involve escape from a co-ordination cage rather than passage from an entrance to a docking site. Thus, the relative rates of dissociation of the three agonists may differ from those of association. Since all three agonists are approximately equivalent in their escape rate constants, it is logical to propose that the quaternary amine moiety of the agonist is the primary determinant of the dissociation rate constant. The ~50-fold difference in the rate constant of dissociation at the two sites (compared with the <5-fold difference in rate constant of association) further suggests that the specific nature of the quaternary amine–protein interaction is substantially different (by about 2·3 kcal mol^{-1}) at $\alpha(\delta)$- and $\alpha(\gamma)$-sites.

Our results indicate that the order of the opening rate constants is ACh > CCh > TMA. Clearly, the nature of the ligand–receptor interaction influences the opening rate constant, with the acetylester group apparently speeding the opening process. We cannot speculate further on the nature of the ligand–receptor interaction that influences the opening rate constant without a more extensive study of other agonists. The closing rate constants of receptors activated by the three agonists were similar but not identical; thus we conclude the nature of the ligand–receptor interaction at the docking site can have a moderate influence on channel closing. However, the free energies of channel closing for the three agonists differ only by about

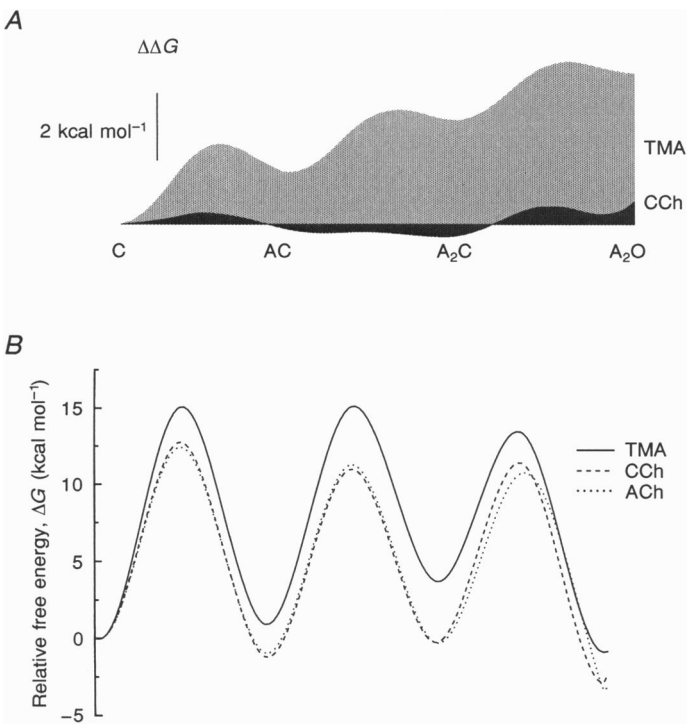

Figure 6. Relative free energy profiles of the activation reaction for ACh-, CCh- and TMA-activated receptors

The rate constants are given in Table 3. *A*, the $\Delta\Delta G$ of each reaction step (relative to ACh). For the endpoints of the reaction, TMA-activated receptors require 5·3 kcal mol^{-1} more energy (70% from the binding steps) than the ACh-activated receptors, whereas CCh-activated receptors require only 0·85 kcal mol^{-1} more energy. *B*, activation free energies (ΔG) of each reaction step. For all agonists, the vacant–closed receptor defines the zero free energy level.

0·5 kcal mol^{-1}, suggesting that other regions of the protein complex are more important determinants of the channel closing rate constant, and/or that at the docking site it is interactions of the quaternary amine with the receptor that determine the rate constant of channel closing.

Summary of results

We have presented three main sets of results regarding recombinant, embryonic-type nicotinic AChR expressed in HEK cells and oocytes. First, ACh binds to the first site (probably the $\alpha(\delta)$-site) more rapidly and with a higher affinity than to the second site. The equilibrium dissociation constants for ACh are ~20 and ~650 μM. In response to a brief, saturating pulse of ACh ~70% of the receptors will open. Second, TMA binds about 100 times more slowly to receptors than does either ACh or CCh, suggesting that non-steric interactions of the agonist molecule with the receptor determine the effective association rate constant. TMA, however, dissociates at about the same rate as ACh and CCh, suggesting that the escape rate constant is determined by interactions of the quaternary amine with the receptor. Because the escape of all three agonists is much faster at the $\alpha(\gamma)$-site, the nature of this interaction is likely to differ at the two binding sites. Third, channel opening rate constants vary substantially with the nature of the agonist. The presence of an ester moiety speeds opening while the channel closing rate constants are only weakly agonist dependent.

Auerbach, A. (1992). ACh receptors subunits in *Xenopus* myocytes activate semi-autonomously. *Biophysical Journal* **61**, A105.

Auerbach, A. (1993). A statistical analysis of acetylcholine receptor activation in *Xenopus* myocytes: stepwise *vs.* concerted models of gating. *Journal of Physiology* **461**, 339–378.

Auerbach, A. & Lingle, C. (1986). Heterogeneous kinetic properties of acetylcholine receptor channels in *Xenopus* myocytes. *Journal of Physiology* **378**, 119–140.

Auerbach, A. & Sachs, F. (1983). Flickering of a nicotinic channel to a subconductance state. *Biophysical Journal* **41**, 1–10.

Ausubel, F. M. (1992). *Protocols in Molecular Biology*, 2nd edn. John Wiley & Sons, Inc., New York.

Ball, F. G. & Sansom, M. S. P. (1989). Ion-channel gating mechanisms: model identification and parameter estimation from single channel recordings. *Proceedings of the Royal Society* B **236**, 385–416.

Blount, P. & Merlie, J. P. (1989). Molecular basis of the two nonequivalent ligand binding sites of the muscle nicotinic acetylcholine receptor. *Neuron* **3**, 349–357.

Case, D. A. & Karplus, M. (1979). Dynamics of ligand binding to heme proteins. *Journal of Molecular Biology* **132**, 343–368.

Chung, S. H., Moore, J. B., Xia, L., Premkumar, L. S. & Gage, P. W. (1990). Characterization of single channel currents using digital signal processing techniques based on hidden Markov models. *Philosophical Transactions of the Royal Society* B **329**, 265–285.

Colquhoun, D. & Sakmann, B. (1985). Fast events in single channel currents activated by acetylcholine and its analogous the frog muscle end-plate. *Journal of Physiology* **369**, 501–557.

Colquhoun, D. & Sigworth, F. J. (1983). Fitting and statistical analysis of single-channel records. In *Single-Channel Recording*, ed. Neher, E. & Sakmann, B. Plenum Press, New York.

Czajkowski, C., Kaufmann, C. & Karlin, A. (1993). Negatively charged amino acid residues in the nicotinic receptor δ subunit that contribute to the binding of acetylcholine. *Proceedings of the National Academy of Sciences of the USA* **90**, 6285–6289.

Forney, G. D. Jr (1972). The Viterbi algorithm. *Proceedings of the IEEE* **61**, 268–278.

Horn, R. (1987). Statistical methods for model discrimination. *Biophysical Journal* **51**, 255–263.

Horn, R. & Lange, K. (1983). Estimating kinetic constants from single channel data. *Biophysical Journal* **43**, 207–233.

Hoshi, T., Zagotta, W. N. & Aldrich, R. W. (1994). *Shaker* potassium channel gating I: Transitions near the open state. *Journal of General Physiology* **103**, 249–278.

Jackson, M. B. (1988). Dependence of acetylcholine receptor channel kinetics on agonist concentration in cultured mouse muscle fibres. *Journal of Physiology* **397**, 555–583.

Jackson, M. B. (1989). Perfection of a synaptic receptor: kinetics and energetics of the acetylcholine receptor. *Proceedings of the National Academy of Sciences of the USA* **86**, 2199–2203.

Kienker, P. (1989). Equivalence of aggregated Markov models of ion-channel gating. *Proceedings of the Royal Society* B **236**, 269–309.

Lingle, C. J., Maconochie, D., & Steinbach, J. H. (1992). Activation of skeletal muscle nicotinic acetylcholine receptors. *Journal of Membrane Biology* **126**, 195–217.

Maconochie, D. J. & Steinbach, J. H. (1992). Adult and foetal acetylcholine receptor channel opening rates. *Biophysical Society Abstract* **61**, A143.

Marshall, C. G., Ogden, D. & Colquhoun, D. (1991). Activation of ion channels in the frog endplate by several analogues of acetylcholine. *Journal of Physiology* **433**, 73–93.

Mody, H. I., Lee, J. & Dilger, J. P. (1994). Activation and block of ACh receptor channels by TMA. *Biophysical Society Abstracts* **66**, A213.

Naranjo, D. & Brehm, P. (1993). Modal shifts in acetylcholine receptor channel gating confer subunit-dependent desensitization. *Science* **260**, 1811–1814.

Pedersen, S. E. & Cohen, J. B. (1990). d-Tubocurarine binding sites are located at δ- and γ-subunit interfaces of the nicotinic acetylcholine receptor. *Proceedings of the National Academy of Sciences of the USA* **87**, 2785–2789.

Roux, B. & Sauve, R. (1985). A general solution to the time interval omission problem applied to single channel analysis. *Biophysical Journal* **48**, 149–158.

Sigworth, F. J. & Sine, S. M. (1987). Data transformations for improved display and fitting of single-channel dwell time histograms. *Biophysical Journal* **52**, 1047–1054.

Sine, S. M. (1993). Molecular dissection of subunit interfaces in the acetylcholine receptor: identification of residues that determine curare selectivity. *Proceedings of the National Academy of Sciences of the USA* **90**, 9436–9440.

Sine, S. M. & Claudio, T. (1991). δ- and γ-subunits regulate the affinity and the cooperativity of ligand binding to the acetylcholine receptor. *Journal of Biological Chemistry* **266**, 19369–19377.

SINE, S. M., CLAUDIO, T. & SIGWORTH, F. J. (1990). Activation of *Torpedo* acetylcholine receptors expressed in mouse fibroblasts. *Journal of General Physiology* **96**, 395–437.

SINE, S. M., QUIRAM, P., PAPANIKOLAOU, F., KREIENKAMP, H.-J. & TAYLOR, P. (1994). Conserved tyrosines in the alpha subunit of the nicotinic acetylcholine receptor stabilize quanternary ammonium groups of agonists and curariform antagonists. *Journal of Biological Chemistry* **269**, 8808–8816.

SINE, S. M. & STEINBACH, J. H. (1987). Activation of acetylcholine receptors on clonal mammalian BC3H-1 cells by high concentrations of agonist. *Journal of Physiology* **385**, 325–359.

TOMASELLI, G. F., MCLAUGHLIN, J. T., JURMAN, M. E., HAWROT, E. & YELLEN, G. (1991). Mutations affecting agonist sensitivity of the nicotinic acetylcholine receptor. *Biophysical Journal* **60**, 721–727.

UNWIN, N. (1993). Nicotinic acetylcholine receptor at 9 Å resolution. *Journal of Molecular Biology* **229**, 1101–1124.

ZAGOTTA, W. N., HOSHI, T. & ALDRICH, R. W. (1994). *Shaker* potassium gating III: evaluation of kinetic models for activation. *Journal of General Physiology* **103**, 321–362.

ZHANG, Y., CHEN, J. & AUERBACH, A. (1994). Single channel kinetics of mouse AChR W57Y. *Biophysical Society Abstracts* **66**, A9.

Acknowledgements

We thank G. Akk and W. Sigurdson for contributing some of the data presented in Table 2, F. Sigworth and R. Horn for generously providing source code that was used in the analysis, K. Lau and M. Teeling for technical assistance, B. Cen and Q. Fu for computer programming, and S. Sine and F. Sachs for discussions and comments on the manuscript. This work was supported by MDA, NIH (NS-23513, and NSF (BIR9015986 and IBN9102232).

Received 29 September 1994; accepted 9 January 1995.